

Dynamic characterization and modification of dynamic properties of a micro scanner

Ilgar Veryeri · Ipek Basdogan

Received: 26 November 2009 / Accepted: 15 March 2010 / Published online: 16 April 2010
© Springer-Verlag 2010

Abstract Micro electro mechanical systems (MEMS) are used in many application areas in different disciplines and took their place among the most promising technologies. The performance of such systems is primarily related to their dynamical characteristics. This study presents the dynamic characterization techniques that are used to identify the modal parameters of a MEMS device and the methods that can be implemented to change its dynamic response. An electrostatic scanner is chosen as the case study to demonstrate the developed methodologies. Initially, the micro scanner is characterized using experimental modal analysis techniques to obtain frequency response function, modal damping, resonance frequencies, and mode shapes. Then, velocity and position feedback control loops are implemented to the scanner system to alter the damping and stiffness characteristics. A closed-loop Simulink model of the scanner is developed to verify the experimental measurements. Several curve fitting methods are used in order to have an accurate representation of the scanner system. Using the model, the influence of both position and velocity feedback on the effective damping, resonance frequency and the transient behavior of the scanner is investigated. The stability limits of the scanner under velocity feedback are also studied via numerical simulations. Based on the experimental and simulation results, the methodology developed in this study proves itself to be very efficient to alter the dynamical

characteristics of the MEMS structures and it can be easily adapted to other MEMS applications.

1 Introduction

Micro scanners are used in many micro electro mechanical systems (MEMS) applications including optical switches, projectors, head-up and head-worn displays, barcode readers and endoscopic cameras. The dynamical characteristics of micro scanners play an important role in the output performance of such systems (Liu et al. 2002; Yalcinkaya et al. 2007; Changho et al. 2006; Urey 2003). The scanning range and frequency, the transient response and the signal to noise ratio are the major performance criteria which in turn may be affected by the stiffness and the damping of the system.

A micro scanner is specifically designed and manufactured based on the requirements of an application. In most of the scanners designed today, electromagnetic, electrostatic, thermal or piezoelectric actuators are used (Houlet et al. 2002; Okano and Hirabayashi 2002; Lin and Fang 2003; Lee et al. 2004; Schweizer et al. 1999; Chau and Dimitrijevic 1999). All of these actuator approaches have their own benefits and drawbacks. However, achieving an optimum design that satisfies both the space constraints and the dynamical requirements of the application is not trivial and still the subject of research. Even if this is achieved, using the same scanner in another application having different dynamical requirements may not be always feasible.

In this study, a comb-drive actuated electrostatic scanner, manufactured by Mirrorcle Technologies Inc. is used as the case study to investigate and modify the dynamical response of the micro structures. The dynamical

I. Veryeri · I. Basdogan (✉)
Mechanical Engineering Department, College of Engineering,
Koc University, 34450 Istanbul, Turkey
e-mail: ibasdogan@ku.edu.tr

characteristics such as the scanning frequency, quality factor and the settling time are among the design parameters of micro scanners that should be highly taken into consideration. For that purpose, a closed loop velocity and position feedback control system is used to modify the effective damping and stiffness characteristics of the scanner. The effect of the velocity and position feedback control system is investigated through experimental and numerical studies.

The methodologies developed to control the effective damping and stiffness of macro systems have recently found many areas of usage in micro and nano systems such as micro gyroscopes, scanning AFM probes, micro resonators and micro scanners (Pannu et al. 2000; Gunev et al. 2007). Some of the reasons for the alteration of the system parameters in micro systems are the fabrication imperfections, external disturbances and necessity for increasing or decreasing the transient response. One of the examples in the literature to overcome fabrication imperfections and subsequently to handle variations in resonance frequency in a micro-resonator is to use an inbuilt sensor and tuner, which are thin films deposited on the hinges of the resonator (Kobayashi et al. 2007). The piezoelectric sensor placed at the hinges of the resonator detects small shifts in resonance frequency. The variations in the frequency are compensated by the tuner, which changes the effective spring constants of the hinges through inverse piezoelectric effect. Since the compensation through the tuner is limited, only small changes are possible. Another study demonstrated that velocity feedback can dramatically improve the dynamic response and external disturbance rejection of an electromagnetic micro-resonator (Nguyen and Howe 1992). The motional current output of the micromechanical resonator is electronically sensed by a sense electrode, converted to a voltage, and then added to or subtracted from the driving input signal to change the effective damping of the resonator. Improving the transient response is another reason for using velocity feedback. For example, in electrophotographic processes, widely used in laser printers where an array of surface micromachined cantilever beams are generally required, velocity feedback is also employed. This approach improves the settling time of the micro beams and reduces the image banding, a type of image artifact due to variations in the velocities of scanners (Cheng et al. 2001). Another example of velocity feedback usage is in electrostatically actuated parallel plate capacitors where low damping may result in long settling times or undesired electrode contact (Palamakumbura et al. 2005). Most of the earlier studies have successfully implemented either position or velocity feedback to change the resonance frequency or the damping characteristics of a micro resonator.

In order to alter the dynamics effectively, one has to first understand the modal characteristics of the scanner. Therefore, before the implementation of the velocity and position feedbacks, the micro scanner is dynamically characterized using experimental modal analysis techniques and the natural frequencies, quality factors and the mode shapes of the system are identified (Veryeri and Basdogan 2007). After the dynamic properties of the micro system are identified, the velocity and position feedback control is implemented and their effect on the frequency and damping characteristics of the system is investigated experimentally and numerically.

In the experimental studies, the velocity of the scanner is directly measured using a Laser Doppler Vibrometer (LDV). The position signal is then obtained through integration. The velocity and position signals are then amplified by adjustable gains through an analog circuit and fed back to the system to change the effective damping and the stiffness of the scanner, respectively. This approach is more robust especially if the nonlinear effects due to friction or external forces significantly influence the output response of the scanner. Under these circumstances, phase shifting and simply scaling the position signal to obtain the velocity signal is not a reliable approach.

In the numerical studies, a Simulink model of the scanner and the velocity and position feedback mechanism is built to verify the experimental results. A transfer function of the scanner is obtained using the experimental frequency sweep data of the first two resonant frequencies. Then, the effect of changing the feedback gains on the dynamic response of the scanner is investigated. The numerical simulations enabled us to explore the system behavior under ideal conditions (free of environmental disturbances) and also determine the range of gain values that are used in the actual experiments.

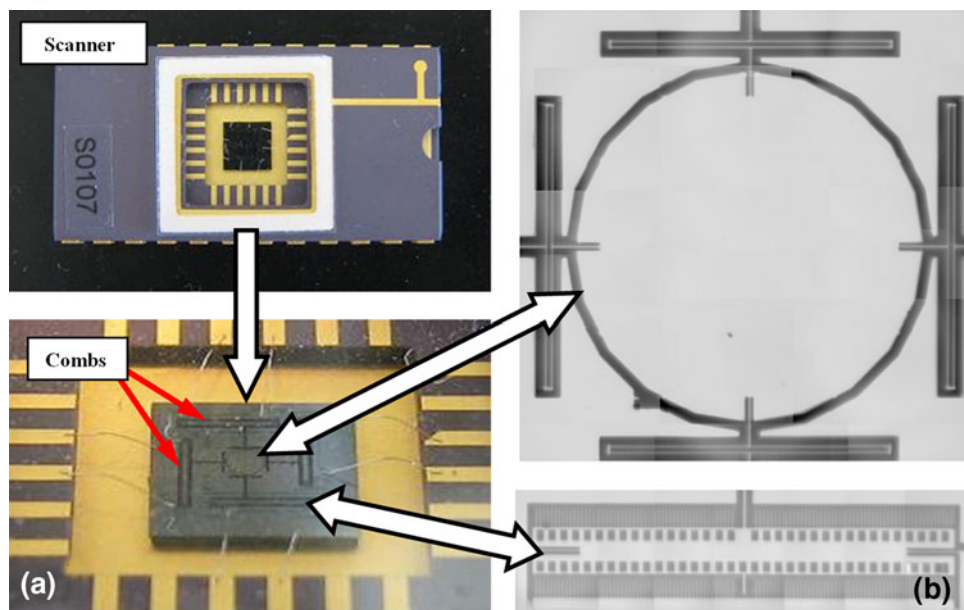
The following section summarizes the fundamental theory including the actuation of the scanner, the feedback methodology and the performance characteristics.

2 Theory

2.1 Actuation principle of the scanner

In this study, a comb-drive actuated scanner is used (Mirrorcle Technologies Inc., model S0107) (see Fig. 1). The actuation is achieved by combs on both fixed and the mobile parts of the actuator. Voltage applied on the system creates electrostatic forces, causing the combs to attract each other. The combs are mostly designed such that the electrostatic forces are linearized with respect to the applied voltages up to a displacement value.

Fig. 1 a Electrostatic scanner’s photo, **b** CCD camera images of the electrostatic scanner and the combs



2.2 Velocity and position feedback control system

When the micro scanner is excited with a sinusoidal torque, it can be modeled as a simple spring-mass-damper system, and its equation of motion can be written as

$$\begin{aligned}
 I\ddot{\theta} + b\dot{\theta} + k\theta &= T_o \cos(\omega t) \\
 \omega_n &= \sqrt{\frac{k}{I}} \\
 Q &= \frac{1}{2\zeta} = \frac{I\omega_n}{b} \\
 \tau &= \frac{1}{\zeta\omega_n} = \frac{2I}{b}
 \end{aligned}
 \tag{1}$$

where θ is the mechanical rotation angle of the mirror, I , b , k and Q are the effective moment of inertia, damping coefficient, and spring constant of the mirror for the n th vibration mode, respectively. ω_n is the natural frequency at that mode and T_o is the amplitude of the external driving torque. The Q factor of a mirror is an indicator of its energy dissipation capacity and is inversely proportional to the damping present in the mirror. A mirror with high Q factor (low damping) dumps its energy slower, resulting in higher-amplitude steady-state oscillations and a sharp resonance curve. On the other hand, low Q factors are desired for improved transient response with shorter settling times (Maithripala et al. 2005). Changes in damping and stiffness of a mirror directly affect its Q -factor and the resonance frequency, respectively. The time constant (τ) is a measure that indicates how fast the system settles within 2% of a certain value. When a velocity and position feedback signal is added to the excitation input, the equation of motion of the system can be written as

$$\begin{aligned}
 I\ddot{\theta} + b\dot{\theta} + k\theta &= T_o \cos(\omega t) + G\dot{\theta} + H\theta \\
 I\ddot{\theta} + (b - G)\dot{\theta} + (k - H)\theta &= T_o \cos(\omega t) \\
 k^* &= (k - H) \\
 \omega_n^* &= \sqrt{\frac{(k - H)}{m}} \\
 Q^* &= \frac{I\omega_n^*}{(b - G)}
 \end{aligned}
 \tag{2}$$

where G and H determine the amount of velocity and position feedback gain, respectively. Equation 2 shows that pure velocity feedback ($H = 0$) only modifies the Q factor of the system, whereas any position feedback leads to the variation of the Q factor as well as the natural frequency, ω_n .

3 Experimental setup

This section summarizes the instruments used in the experiments (see Fig. 2) and their main functions. In the feedback circuit part, the circuit elements are as follows.

3.1 Function generator

Agilent 33220A is a 20 MHz synthesized function generator (signal generator) with built-in arbitrary waveform and pulse capabilities.

3.2 Laser Doppler vibrometer

The scanner’s vibrational out-of-plane velocity is measured by Polytec Fiber Optic Vibrometer (Polytec Datasheet) operating based on the Doppler principle, detecting

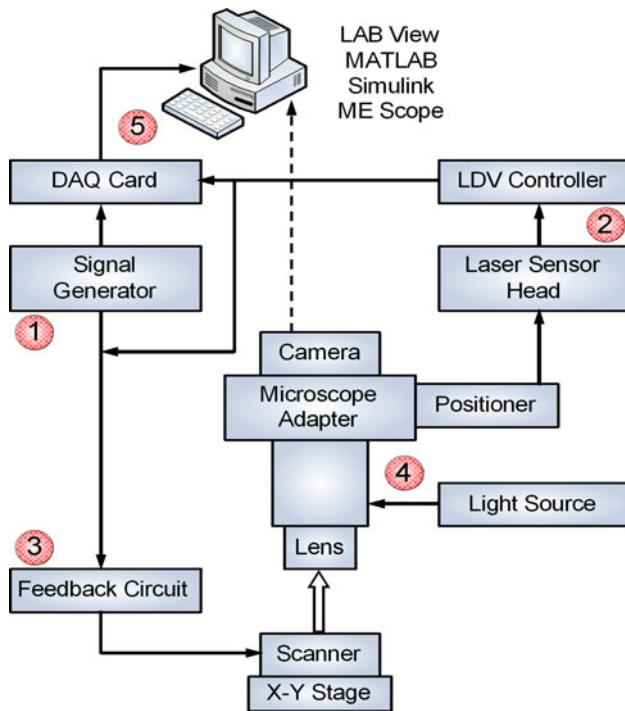


Fig. 2 Schematic of the experimental setup

back-scattered laser light from a vibrating structure. The LDV consists of the OFV-551 fiber interferometer and the OFV-5000 vibrometer controller.

3.3 Feedback circuit

The mirror is actuated using a velocity and position feedback circuit as shown in Fig. 3. The components of the feedback circuit are the phase shifter, the voltage follower, the integrator and the gain amplifiers. The circuit components are as follows.

3.3.1 Phase shifter

The analog phase shifter is integrated into the signal processing circuit to adjust the phase deviations at different frequencies due to the intrinsic time delay in the LDV. Obtaining a true velocity signal with 0° or 180° phase shift is necessary to feed the signal back to the system properly.

In the phase shifter, STMicroelectronics wide bandwidth operational amplifier LF-351 is used (see Fig. 4). The resistances ‘R1’ and ‘R2’, connected to the operational amplifier determine the input to output amplitude ratio. If the amplitude ratio is to be kept constant, ‘R1’ and ‘R2’ values should be taken the same and high enough to reduce the error.

The amount of shift can be tuned by adjusting the capacitance ‘C1’ or the resistance ‘R3’ in the phase shifter circuit (see Fig. 4). The resistance and capacitance values are designed using *pSpice* circuit design program. After selecting a value for the capacitance, the resistance can be fine tuned in its allowable range to obtain a desired shift in phase at a specific frequency.

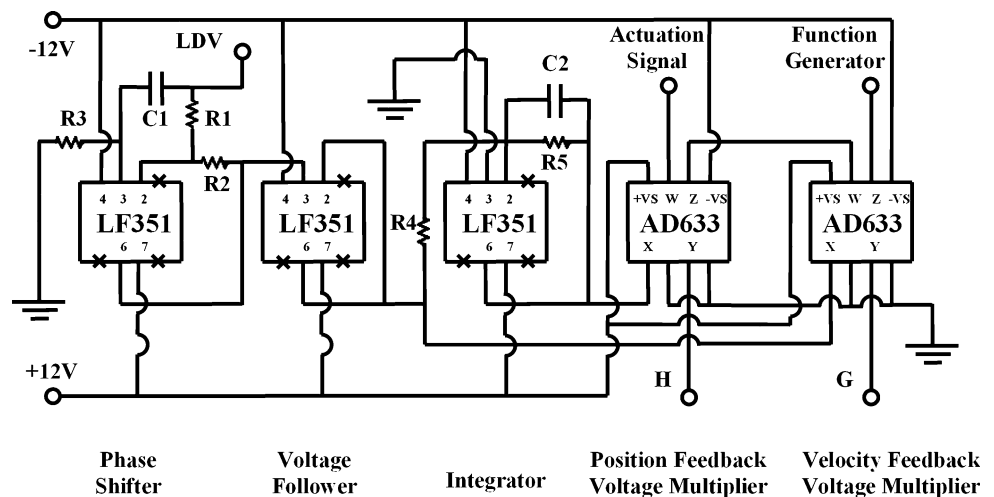
3.3.2 Voltage follower

In some conditions, due to high impedance, the current at some points becomes too small. To overcome this problem, a voltage follower is placed at the output of the phase shifter (see Fig. 3). A voltage follower is again an operational amplifier (LF351) which outputs a low impedance voltage that is identical to its input. The enhanced velocity signal is sent both to the integrator and the velocity feedback gain amplifier.

3.3.3 Integrator

For a real integration process, the phase of a sinusoidal signal should be shifted 90° while the amplitude should be

Fig. 3 The velocity and position feedback circuit



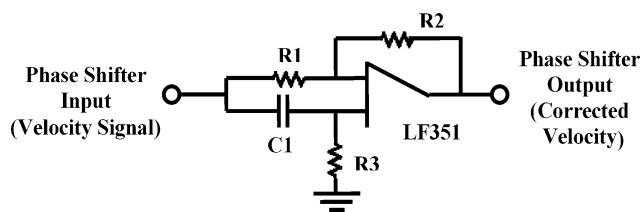


Fig. 4 The phase shifter part of the circuit

reduced by an amount of the working frequency. Therefore, for a system having a resonant frequency in the orders of kHz, the integrated signal will be practically too small to observe. However, if that signal will be used for feedback purposes, a scaling factor in the integration process will be needed in order to maintain the integrator output to input ratio (O/I ratio) close to unity. In the integrator component (see Fig. 5), the operational amplifier LF351 is used to modify the phase shifter’s output signal.

The *pSpice* software is used to select the right resistance and capacitance values for the integrator component of the circuit. The capacitor ‘C2’ and two resistors ‘R4’ and ‘R5’ affect both the amplitude and the phase simultaneously. Having analyzed the effects of the varying the values of the resistances and the capacitance, the appropriate values for the components are selected.

3.3.4 Velocity feedback voltage amplifier

The voltage amplifier used in the feedback loops is Analog Devices, Analog Multiplier AD633. The scale factor of 10 V is provided by a buried Zener diode in the analog multiplier.

Fig. 5 The integrator part of the circuit

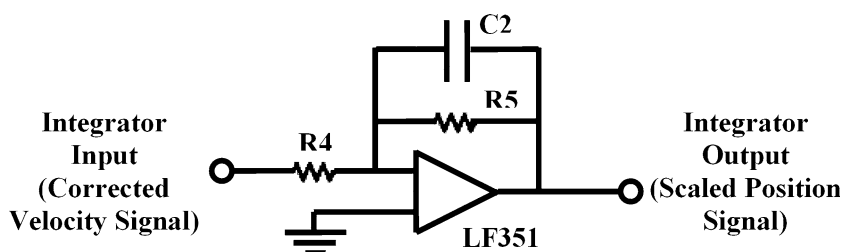
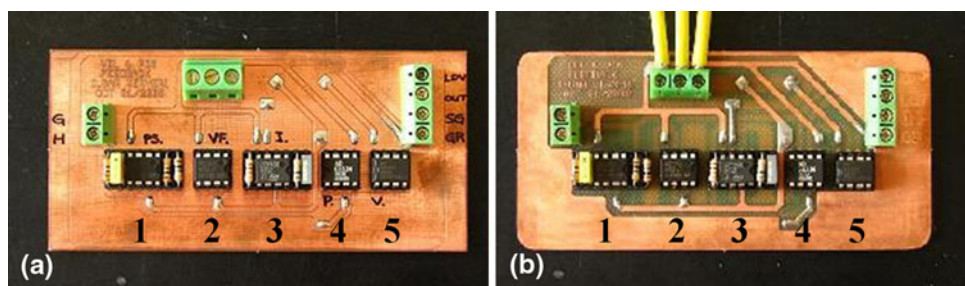


Fig. 6 a The original PCB, b the engraved PCB (1 phase shifter, 2 voltage follower, 3 integrator, 4 position feedback voltage amplifier, 5 velocity feedback voltage amplifier)



3.3.5 Position feedback voltage amplifier

The generated output of the velocity feedback voltage amplifier is the summing input of the position feedback voltage amplifier. Similarly, the multiplication of the position signal received from the integrator with the position gain H is then added to this summing input. The existence of two separate feedback elements allows to feedback the system both with velocity and position data independently.

3.3.6 Circuit board

The final configuration of printed circuit board (PCB) is shown in Fig. 6.

3.4 Microscope system

Focusing and image capturing processes are performed in the microscope system. It is composed of five main parts, being VM-1V Video adaptable microscope, Meiji-S.Plan objectives, Meiji FL150 light source with halogen lamp, a CCD camera and a Polytec microscope scan unit MSV-50 (Polytec User Manual). The Polytec microscope scan unit is composed of two main parts which are OFV-71 and OFV-72. OFV-72 is the microscope adapter for the camera and OFV-71 is the manual positioner for the laser beam.

4 Implementation of velocity and position feedback control

In this section, the results of the experiments are presented. The voltage limitations of the electrostatic scanner are

tested prior to the feedback experiments (see Sect. 4.1). The dynamic characterization of the scanners is performed in Sect. 4.2, and then the velocity and position feedbacks are implemented to change the damping and frequency characteristics of the scanner.

4.1 Behavior of the scanner under sinusoidal voltages

The electrostatic scanner requires a sinusoidal input voltage combined with a DC voltage. The reason for this is that the scanner is a one-quadrant device which is able to deflect from rest position to one side only, but not to the opposite side. Hence, only the positive excitation signals can drive the scanner. In experiments, it is critical that the sinusoidal input amplitudes always lie under the DC voltage amplitude. The output response for increasing sinusoidal voltage with constant DC offset at the resonant frequency is plotted (see Fig. 7). As it can be observed from Fig. 7, the scanner velocity changes linearly as a function of input voltage and does not become bounded even at the high voltages.

4.2 Dynamic characterization of the scanner

In order to alter the dynamics of effectively, the modal characteristics of the scanner must be well-understood. For that purpose, before implementing the velocity and position feedback control, we dynamically characterized the micro scanner using experimental modal analysis techniques and identified the natural frequencies and the mode shapes of the system. Dynamic characterization technique of the micro systems and part of the experimental system used in

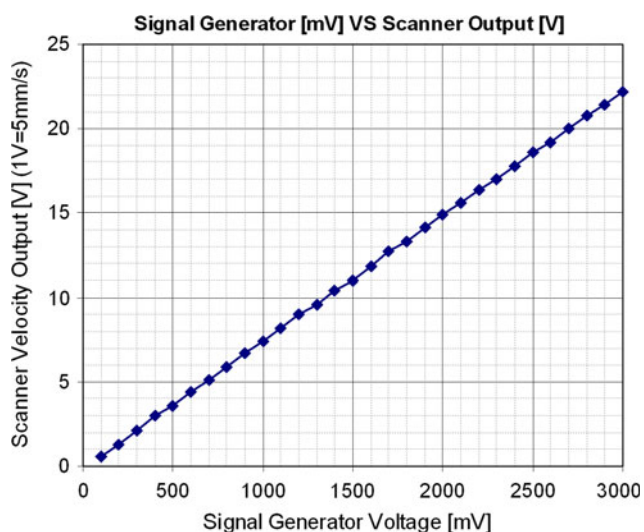


Fig. 7 Amplitude of the electrostatic scanner velocity as function of input voltage

this study was developed in an earlier study (Anac and Basdogan 2008).

The exact locations of the data points are required for the repeatability of the experiments. On that account, the images captured from the surface of an individual scanner are initially combined to obtain the whole surface image. That surface image is then divided by grids and made transparent to prepare a ghost image (see Fig. 8). The real time CCD camera image is finally matched to a suitable position on that ghost image by MATLAB (see Appendix B for the MATLAB code). This operation enables us to direct laser beams on the desired locations of the grid surface.

After the voltage limitation of the scanner is determined, the scanner is actuated by applying sinusoidal excitation voltage within a safe range. Frequency response characterization is done by sweeping the frequency of the excitation signal while keeping the amplitude constant. The frequency response function of the point 17 is given in Fig. 9. Note that, the translational motion of the grid nodes are measured, rather than the rotational motion. With the assumption of the small scanning angles, it corresponds to an error at a level of 0.5%.

Throughout the sweep, the frequency, velocity amplitude of the scanning point and the phase difference between the input and output signals are recorded to obtain the frequency response curves of predefined grid locations. Driving the scanner via the signal generator, the data acquisition and recording processes are performed by a LABVIEW interface program.

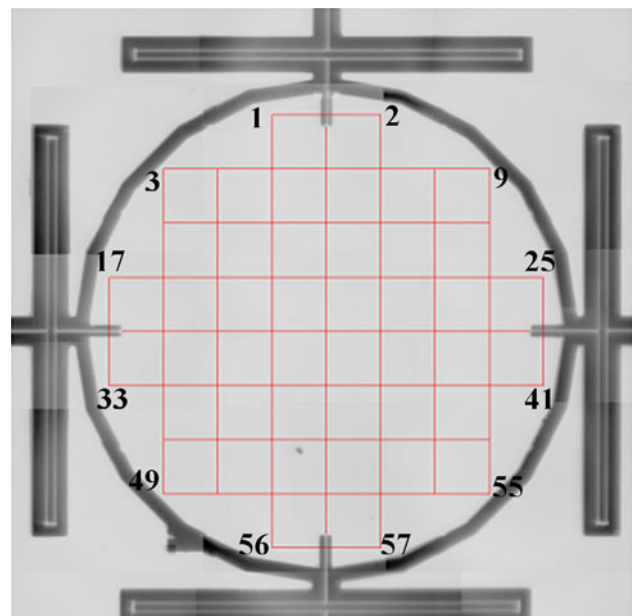
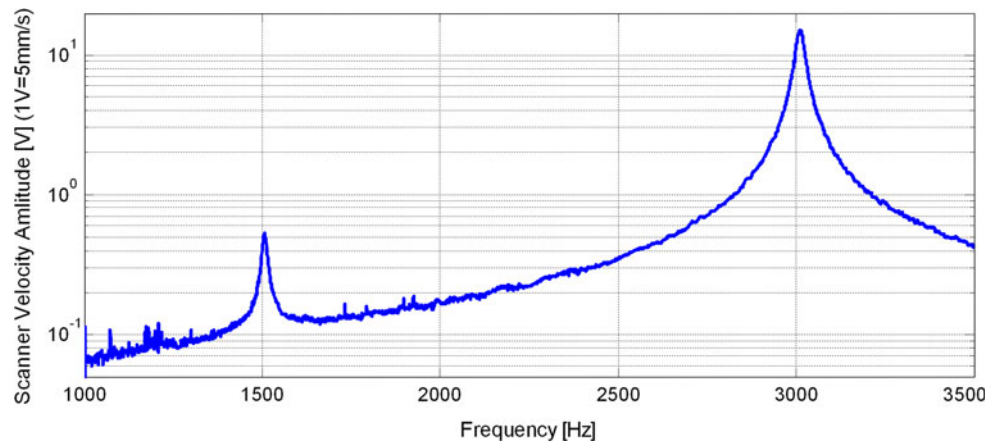


Fig. 8 MATLAB Ghost images with grid Electrostatic scanner

Fig. 9 Frequency response function of the electrostatic scanner (Point 17, under 1 V sinusoidal input excitation with 2 V DC offset)



After the amplitude and the phase difference information are recorded for all the points on the grid, they are converted into real and imaginary parts as an input to the ME'Scope program for the mode characterization (ME'Scope Manual 2001). A surface model of the scanner is also built to visualize the mode shapes. The measurement data is mapped to the related points on the surface model. The program uses integrated curve fit techniques to match a model to the experimental frequency response functions. Finally, the modal analysis is performed to estimate the mode shape and the modal parameters for the second resonance mode.

The torsional mode of the electrostatic scanner is shown in Fig. 10. Note that, the damping ratio, ζ calculated by ME'Scope is also consistent with the Q -factor calculated using the *half power point method* where $Q \cong \frac{\omega_n}{\omega_2 - \omega_1}$ (Rao 2004).

4.3 Velocity feedback

To observe the effect of the change in velocity gain G to the dynamical characteristics, frequency response curves for discrete G values are plotted for the scanner (see Fig. 11). The quality factors and time constants are calculated from the receptance graphs (displacement per input

excitation) and their percent changes with respect to G are plotted in Fig. 12. As seen from the plots, Q and τ are increasing with increasing G , while G barely has an effect on the resonance frequency, as expected from Eqs. 1 to 2.

One should notice that, the scanner becomes unstable beyond the velocity gain $G = 0.07$. It was observed that, the quality factor of the electrostatic scanner can be increased by a factor of approximately ten times the initial value.

4.4 Position feedback

Similarly, to see the influence of the position gain H , frequency response curves under different H gain voltages are plotted. As one can notice, the voltages required for position feedbacks are more than the required voltages for the velocity feedbacks. The electrostatic scanner results for position feedback are plotted in Fig. 13.

After the quality factors and time constants are calculated from the receptance graphs, their percent changes and the frequency shifts with respect to H are plotted in Fig. 14. Recalling from the theory described in Sect. 2.2, for a second order system under pure position feedback, as long as only the stiffness is affected, the time constant should remain constant and the quality factor should stay linearly

Fig. 10 ME'Scope torsional mode representation of electrostatic scanner (ME'Scope)

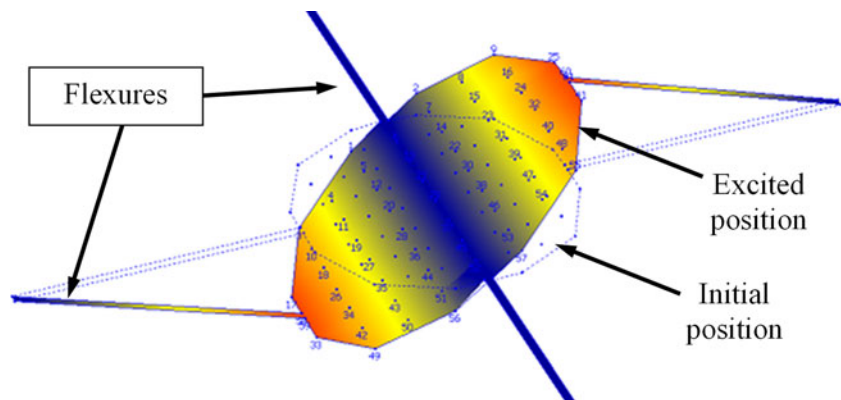


Fig. 11 Experimental frequency response curves for different G values under 80 mV sinusoidal input excitation

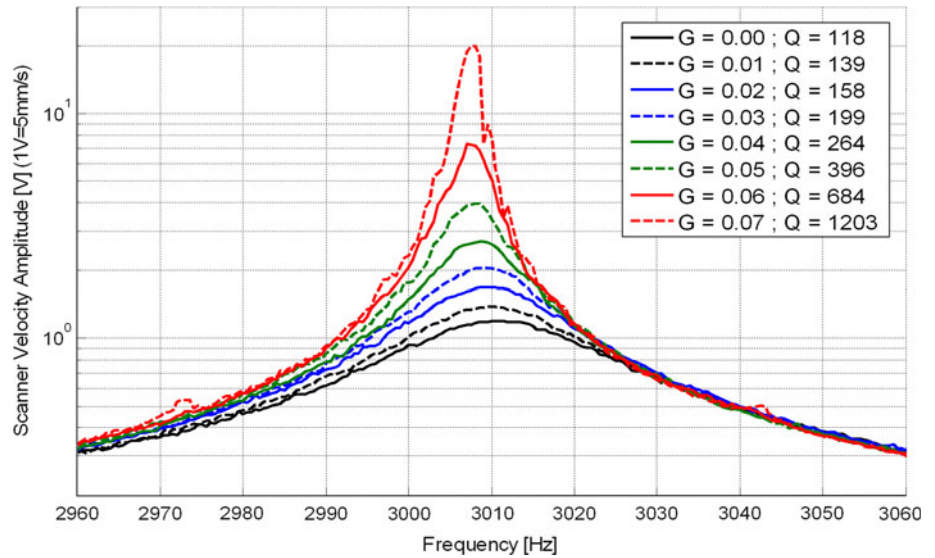


Fig. 12 Percent change in **a** quality factor, **b** time constant, for different G values

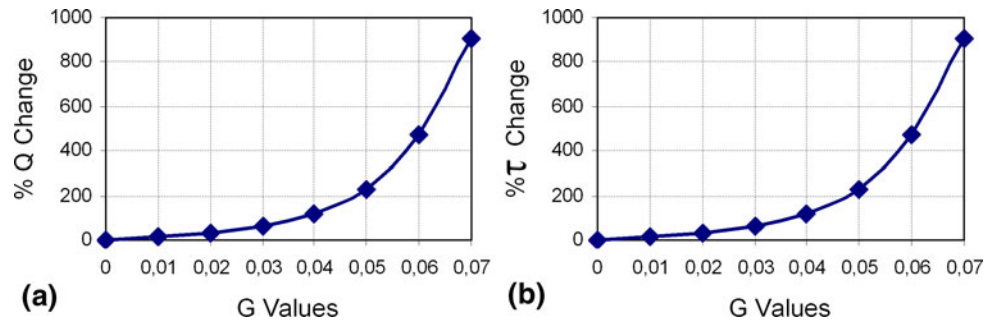
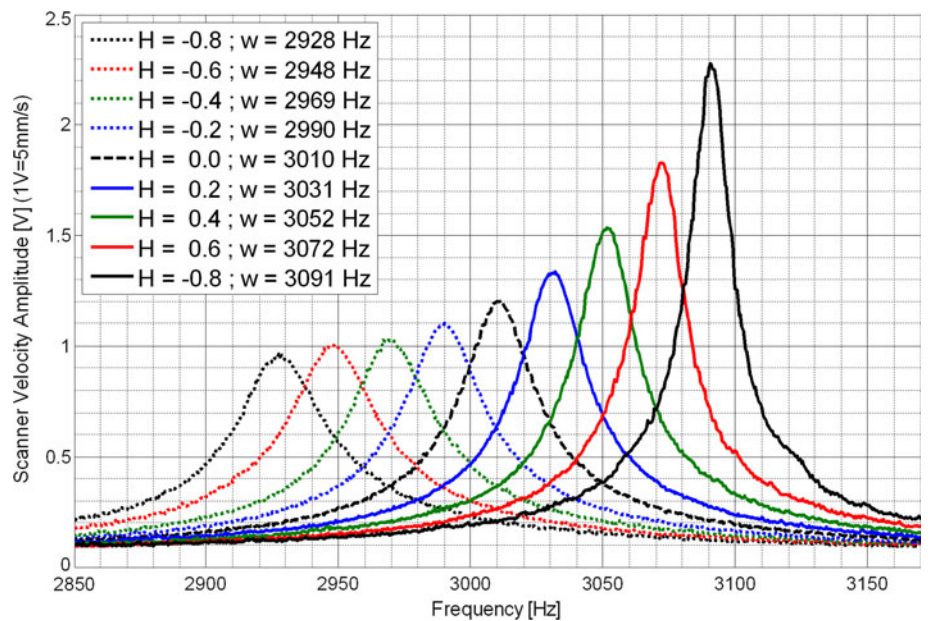


Fig. 13 Experimental frequency response functions for different H values (electrostatic scanner, under 80 mV sinusoidal input excitation)



proportional with the natural frequency. However, the system does not behave as a second order system under position feedback. As seen from the plots, the time constant is increasing with increasing H gain. Moreover, while the

resonance frequency shifts almost linearly with the H gain, the quality factor's increase is not linear because of the change in the time constant. This unexpected phenomenon can be explained by the frequency change of all other

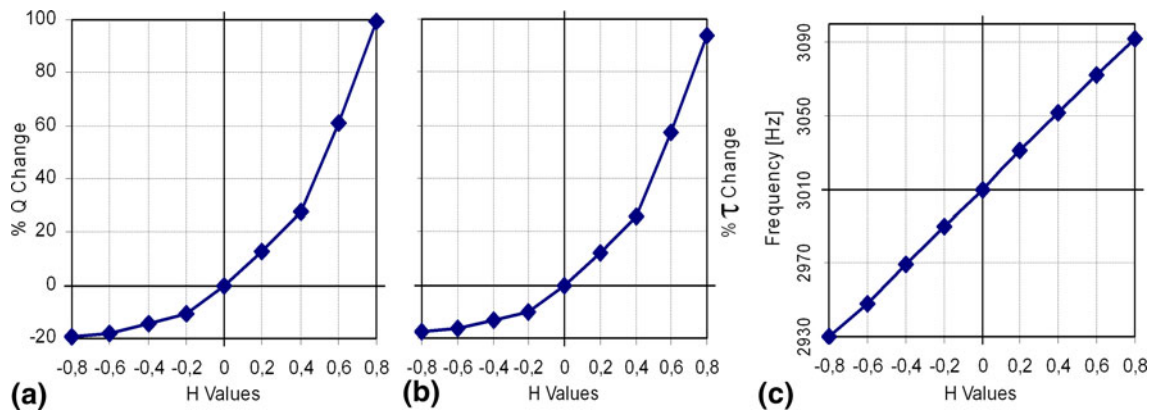


Fig. 14 Percent change in **a** quality factor, **b** time constant and **c** the shift in resonance frequency, for different *H* values

modes, forcing the scanner not to act as a second order system.

4.5 Concurrent feedback

To see the feasibility of concurrent feedback, both velocity and position feedbacks are introduced into the system together. It is demonstrated that by adjusting the gains independently, it is possible to carry the resonance to a desired frequency and change the damping of the system simultaneously (see Fig. 15).

4.6 Stability analysis from FRFs

The system under velocity feedback can be represented as in Fig. 16, where *G* is the velocity gain and *T*(*s*) is the open-loop transfer function between the input voltage ‘inp(*s*)’ and the output velocity voltage ‘out(*s*)’ (see Eq. 3).

Frequency response functions are obtained by the steady-state response of the system at discrete frequency values and are used to represent the transfer function describing the sinusoidal steady-state behavior. To convert the system into frequency domain, *s* is replaced with the complex variable *iω* (see Eq. 4).

$$T(s) = \frac{\text{out}(s)}{\text{inp}(s)} \Big|_{G=0} \tag{3}$$

$$T(i\omega) = \frac{\text{out}(i\omega)}{\text{inp}(i\omega)} \Big|_{G=0} = \frac{|\text{out}(\omega)|e^{i\phi_{\text{out}}(\omega)}}{|\text{inp}(\omega)|e^{i\phi_{\text{inp}}(\omega)}} \Big|_{G=0} \tag{4}$$

$$\frac{\text{out}(i\omega)}{\text{inp}(i\omega)} = \frac{T(i\omega)}{1 - T(i\omega)G} \tag{5}$$

According to the closed loop transfer function, we require *T*(*iω*)*G* < 1 for the stability criteria (see Eq. 5). The *G* gain values where the system becomes unstable change with the frequency. Hence, to find the maximum

Fig. 15 Concurrent feedback results for the electrostatic scanner

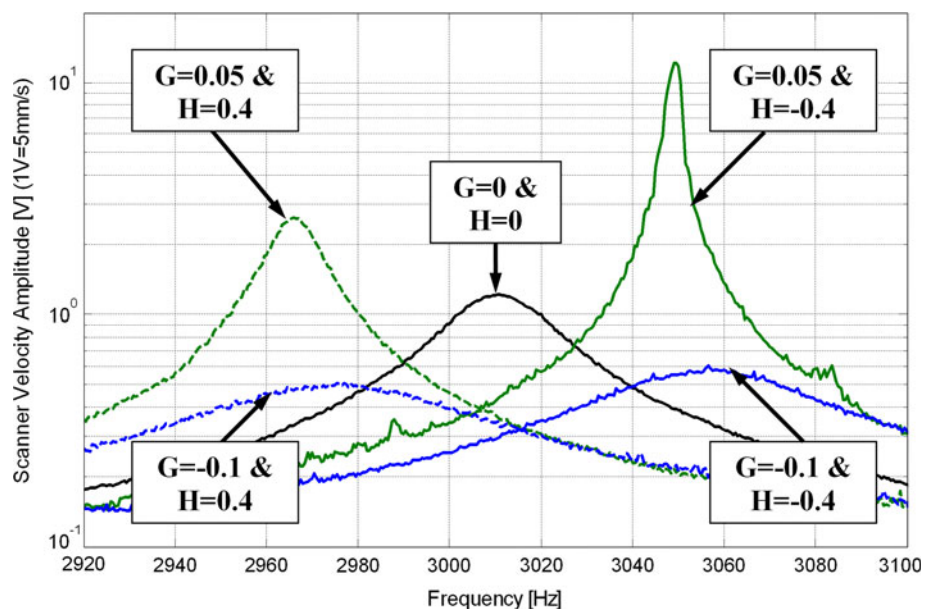
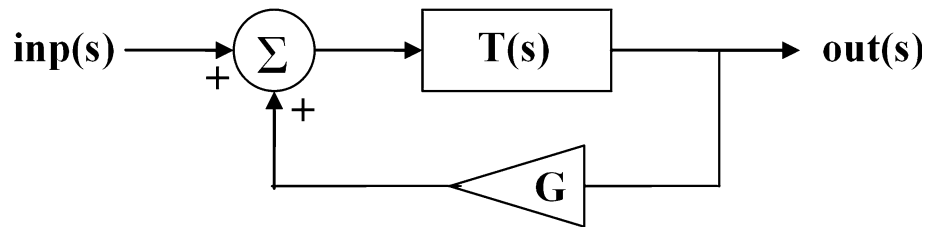


Fig. 16 Velocity feedback block diagram



gain value safely applicable to the system for all frequencies, the minimum possible gain should be selected. Since $T(i\omega)$ and G are inversely proportional, the critical G value can be attained at the resonance frequency, where $T(i\omega)$ is at its maximum. At the resonance frequency, the phase difference between the input and output voltage is an integer multiple of 180° by definition. Knowing that the phase of the input signal must be 0° , the maximum gain value is found to be the magnitude ratio of the input to the output at the resonance frequency (see Eqs. 6–8).

$$\phi_{\text{inp}(\omega)} = 0^\circ \rightarrow e^{i\phi_{\text{inp}(\omega)}} = 1 \tag{6}$$

$$\phi_{\text{inp}(\omega_N)} = n \cdot 180^\circ \rightarrow e^{i\phi_{\text{out}(\omega_N)}} = (-1)^n \tag{7}$$

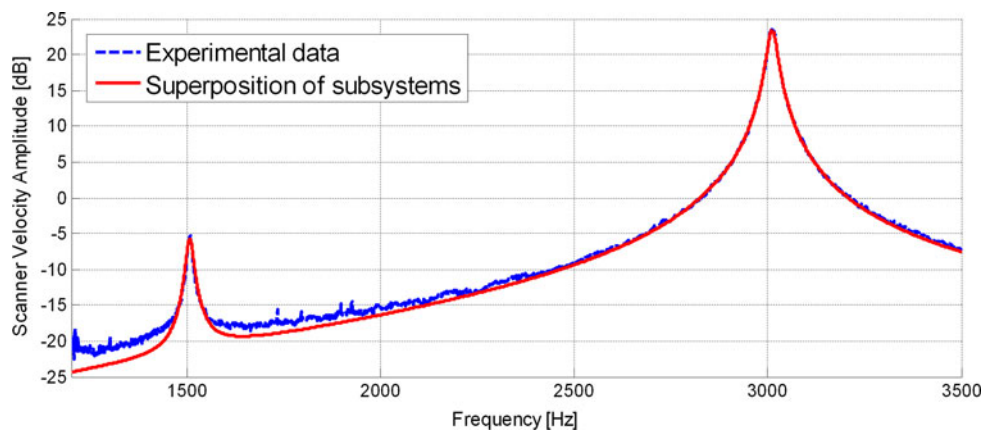
$$G < \frac{1}{T(i\omega)} = \frac{|\text{inp}(\omega_N)| e^{i\phi_{\text{inp}(\omega_N)}}}{|\text{out}(\omega_N)| e^{i\phi_{\text{out}(\omega_N)}}} = (-1)^n \cdot \frac{|\text{inp}(\omega_N)|}{|\text{out}(\omega_N)|} \tag{8}$$

From Eq. 8, the maximum possible G value for the scanner is found to be 0.067. This result agrees with the experimental gain limit which was found to be 0.071 (see Fig. 11).

5 Simulation results and comparison

In this section, Simulink model of the micro scanner and the integrated feedback loops are developed to verify the experimental measurements. The effect of velocity and position feedback loop variables on the dynamical behavior of the scanner is investigated.

Fig. 17 Superposition of subsystems fit to the experimental data of the electrostatic scanner under 1 V sinusoidal input excitation with 2 V DC offset



5.1 Construction of the simulation model

The transfer function of the system is obtained by the superposition of two-second order polynomials (one for each resonance frequency), and a delay. After the first two resonance frequencies of the scanner ($\omega_1 = 1,507$ Hz and $\omega_2 = 3,010$ Hz) are obtained from the amplitude plots and the quality factors are calculated using the half-power method around the resonance peaks, the first and second order terms of the polynomials are calculated using the corresponding peak's dynamical characteristics. These two transfer functions are superimposed and a delay is introduced in the model in order to fine tune the resultant transfer function to obtain the desired shifts in phase at the resonance frequencies (Fig. 17). Then the velocity and position feedback mechanisms are integrated with the micro-scanner model to simulate the response of the whole system. The velocity and position gains, G and H are varied to investigate the effect of feedbacks gains on the dynamical characteristics of the scanner (see Fig. 18).

5.2 Velocity feedback comparison

As shown in Fig. 19, the response of the Simulink model is very close to experimental results for different gain values. It should be recalled that the resonance frequencies under pure velocity feedback must remain unchanged, as in the case with simulation curves. Yet, slight shifts in the experimental resonance peaks are noticed for increasing G values (3 Hz maximum). In spite of the fact that there are

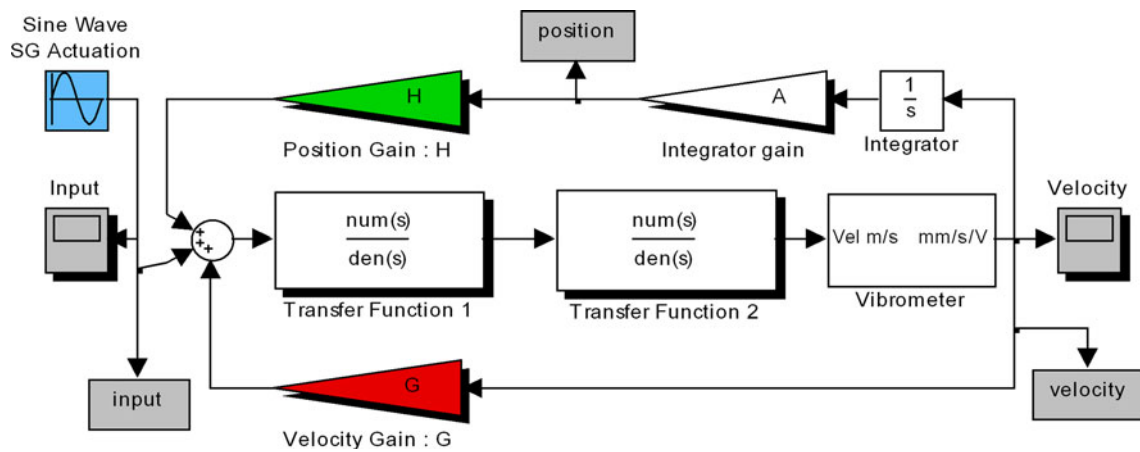
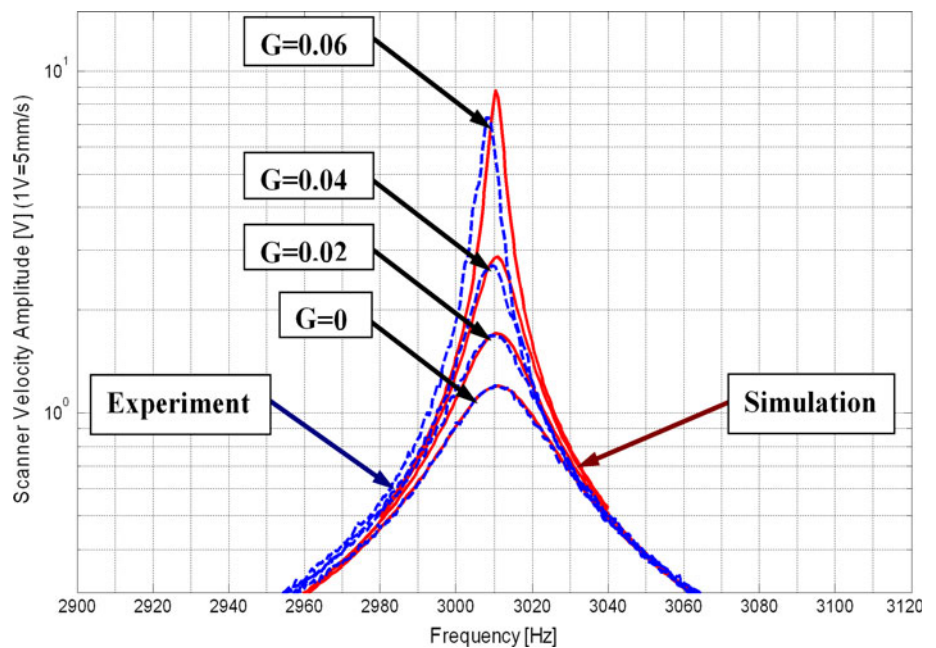


Fig. 18 Simulink model with feedback loops

Fig. 19 Velocity feedback comparison



small discrepancies due to that shift, the curves are reasonable even for greater values of G gains. The response curves are plotted up to $G = 0.06$, since the simulation results show that the system become unstable at $G = 0.067$. This result obtained from the simulation also agrees with the stability limit obtained through the analytical method which was explained in Sect. 4.6.

5.3 Position feedback comparison

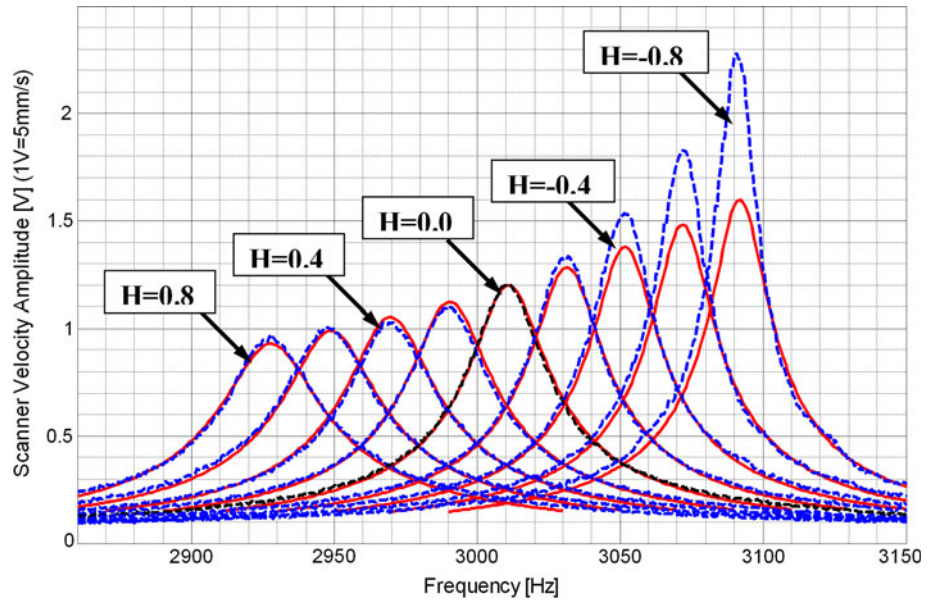
It is observed that when the position feedback mechanism is on, the second peak’s resonance frequency is decreased and the resonance curves are approaching to each other as the gain H is increased, and vice versa. The second important behavior to notice is that the amplitudes of

approaching curves are decreasing (see Fig. 20). The change in the amplitudes with altering frequency is the result of the neighboring resonance peak. Also it is observed that the simulation results differ from the experimental ones in terms of amplitudes at the higher frequencies. This may be due to the assumptions made while building the Simulink model. The superposition model may not be capturing the whole dynamics of the micro-system.

5.4 Concurrent feedback and dynamic characteristics analysis

The advantage of having two feedback loops is that once the resonance frequency is set, the effective damping of the system can be altered independently by adjusting the

Fig. 20 Position feedback curves (*dashed lines* experimental data, *solid lines* simulation data)



gain G . By adjusting both the position and velocity gains, the resonance frequency and the damping characteristics of the system were proven to be set simultaneously. Because of the fact that there are slight frequency shifts in the experimental velocity feedbacks, there is a slight discrepancy between the numerical and simulation results (see Fig. 21).

To see the percent changes in quality factor and time constant, a list of test cases altering G and H gains is tabulated in Table 1. One can notice that, changing the gain G has a major influence on both quality factor and time constant, while it has no influence on any of the resonance frequencies which are altered by H gains. Unfortunately, there is always a trade-off between quality factor and the

time constant. Even though there are some regions where both the quality factor and the time constant are improved, their percent changes are extremely insignificant. Considering this fact, the gain G has to be adjusted depending on the application priorities. In stability limits of the scanner, a quality factor improvement of almost 2,400% or a decrease in settling time by 60% is observed.

Due to the coupling of vibration modes, the alterations in the gain H have an influence on every system characteristics, in some degree. For greater G gains, remarkable changes are observed in quality factor and time constant, along with the change of the H gains. As G gains decrease, especially for its negative values, the influence of H gains over damping characteristics become insignificant.

Fig. 21 Concurrent feedback results (*dashed lines* experimental data, *solid lines* simulation data)

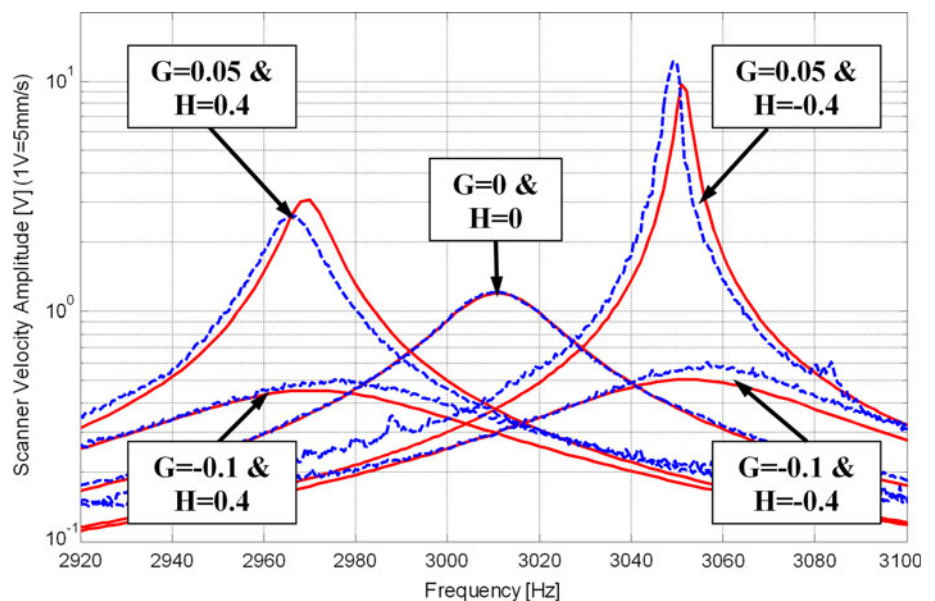


Table 1 Percent changes in peak amplitude, quality factor and time constant for different values of G and H gains for the electrostatic scanner

H : Freq (Hz):	0.8 2,928	0.6 2,949	0.4 2,970	0.2 2,991	0 3,011	-0.2 3,032	-0.4 3,052	-0.6 3,072	-0.8 3,092
$G = 0.06$									
V_{\max} (V)	3.07	3.82	4.99	7.08	11.18	33.72	–	–	–
$\% \Delta Q$	150.3	210.5	307.0	484.3	781.4	2,393	–	–	–
$\% \Delta \tau$	157.4	217.1	312.7	488.2	781.4	2,376	–	–	–
$G = 0.04$									
V_{\max} (V)	1.74	1.95	2.22	2.56	2.99	3.58	4.40	5.65	7.83
$\% \Delta Q$	41.2	60.1	83.2	113.4	150.0	197.5	266.0	373.7	551.2
$\% \Delta \tau$	45.3	63.5	85.7	114.9	150.0	195.5	261.1	364.3	534.1
$G = 0.02$									
V_{\max} (V)	1.21	1.31	1.43	1.56	1.71	1.89	2.10	2.35	2.66
$\% \Delta Q$	-1.6	7.4	17.6	29.8	42.9	57.7	76.9	101.0	128.2
$\% \Delta \tau$	1.2	9.7	19.3	30.7	42.9	56.6	74.5	97.0	122.2
$G = 0$									
V_{\max} (V)	0.93	0.99	1.05	1.12	1.20	1.28	1.38	1.48	1.60
$\% \Delta Q$	-24.5	-19.2	-13.4	-7.1	0.0	7.7	16.6	26.3	30.9
$\% \Delta \tau$	-22.4	-17.5	-12.2	-6.5	0.0	7.0	15.0	23.8	27.5
$G = -0.02$									
V_{\max} (V)	0.76	0.79	0.83	0.88	0.92	0.97	1.03	1.08	1.14
$\% \Delta Q$	-38.6	-35.1	-31.3	-27.2	-22.8	-18.2	-13.0	-7.6	-1.8
$\% \Delta \tau$	-36.9	-33.7	-30.3	-26.8	-22.8	-18.8	-14.2	-9.4	-4.4
$G = -0.04$									
V_{\max} (V)	0.64	0.66	0.69	0.72	0.75	0.78	0.82	0.85	0.89
$\% \Delta Q$	-48.2	-45.6	-42.9	-40.1	-37.2	-33.9	-30.6	-27.3	-23.7
$\% \Delta \tau$	-46.7	-44.4	-42.1	-39.7	-37.2	-34.3	-31.6	-28.8	-25.7
$G = -0.06$									
V_{\max} (V)	0.55	0.57	0.59	0.61	0.63	0.65	0.68	0.70	0.73
$\% \Delta Q$	-55.5	-53.6	-51.7	-49.7	-47.6	-44.9	-42.2	-40.0	-37.9
$\% \Delta \tau$	-54.2	-52.6	-51.0	-49.3	-47.6	-45.3	-43.0	-41.2	-39.5
$G = -0.08$									
V_{\max} (V)	0.48	0.50	0.51	0.53	0.55	0.56	0.58	0.60	0.62
$\% \Delta Q$	-60.7	-59.3	-57.7	-56.0	-54.2	-52.4	-50.7	-49.0	-47.2
$\% \Delta \tau$	-59.6	-58.4	-57.1	-55.7	-54.2	-52.7	-51.4	-50.0	-48.6
$G = -0.10$									
V_{\max} (V)	0.43	0.44	0.45	0.47	0.48	0.49	0.51	0.52	0.53
$\% \Delta Q$	-64.8	-63.6	-62.5	-61.2	-59.9	-58.4	-57.1	-55.8	-54.1
$\% \Delta \tau$	-63.8	-62.9	-61.9	-61.0	-59.9	-58.7	-57.7	-56.7	-55.3

Meanwhile, the resonance shifts stays generally linear with H and are independent of G . Therefore, it is important to set the working frequency prior to the adjustment of G gains.

6 Conclusion and discussion

In this study, the effective damping and stiffness of an electrostatic micro scanner is adjusted experimentally

using a feedback circuit. In our approach, the velocity of the scanner is measured directly using a LDV. Obtaining the velocity signal from the measured position signal through differentiation is not preferred since the noise in the position signal is amplified in the process; instead the velocity signal is integrated and scaled to obtain a cleaner position signal. The velocity and position signals are first multiplied by separate gains and then added to the driving signal to change the effective characteristics of the micro scanner system. With this approach, the resonance

frequency of the scanner or damping of the structure can be altered in real-time.

Simulink model of this scanner is also developed from experimental data to investigate the influence of both position and velocity feedback on the resonance frequency, damping and the settling time of the scanners is investigated. Having a numerical model of the system and feedback loops was very helpful for estimating the system behavior and the stability range of velocity gain values that can be used in the real experiments. The overall study showed that coupling effects can significantly influence the response of the scanners as the position feedback gain H is altered. Due to this effect, H also manipulates the damping characteristics, in addition to the resonance frequency. The effect of concurrent feedback on dynamical characteristics of the system is also analyzed. In general, the velocity gain G is the major factor that affects the quality factor and the time constant of the system. There is a trade-off between the quality factor and the settling time, though. While decreasing values of G reduces the time constant of the system, it also reduces the quality factor, hence the amplitude of oscillations.

References

- Anac O, Basdogan I (2008) Model validation and performance prediction in the design of micro systems. *J Vib Control* 14(11):1711–1728
- Changho C, Keiji I, Hiroshi T (2006) Optically modulated MEMS scanning endoscope. *IEEE Photon Technol Lett* 18(1–4):133–135
- Chau KH, Dimitrijević S (1999) Two-dimensional microscanner actuated by PZT thin film. *SPIE Proc Device Process Technol MEMS Microelectron* 3892:133–140
- Cheng HM, Ewe MTS, Chiu GTC, Bashir R (2001) Modeling and control of piezoelectric cantilever beam micro-mirror and micro-laser arrays to reduce image banding in electrophotographic processes. *J Micromech Microeng* 11:487–498
- Günev I, Varol A, Karaman S, Basdogan C (2007) Adaptive Q control for tapping-mode nanoscanning using a piezoactuated bimorph probe. *Rev Sci Instrum* 78(4):043707.1–8
- Houlet L, Helin P, Bourouina T, Reyne G, Gergam ED, Fujita H (2002) Movable vertical mirror arrays for optical microswitch matrixes and their electromagnetic actuation. In: Solid-state sensor, actuator and microsystems, Workshop Hilton Head Island, South Carolina
- Kobayashi T, Maeda R, Itoh T, Sawada R (2007) Smart optical microscanner with piezoelectric resonator, sensor, and tuner using $\text{Pb}(\text{Zr}, \text{Ti})\text{O}_3$ thin film. *Appl Phys Lett* 90:183514
- Lee D, Krishnamoorthy U, Yu K, Solgaard O (2004) Single crystalline silicon micromirrors actuated by self aligned vertical electrostatic comb drives with piston motion and rotation capability. *Sens Actuators A* 114:423–428
- Lin HY, Fang W (2003) A Rib-reinforced micro torsional mirror driven by electrostatic torque generators. *Sens Actuators A* 105:1–9
- Liu AQ, Zhang XM, Murukeshan VM, Zhang QX, Zou QB, Uppili S (2002) An optical crossconnect (OXC) using drawbridge micromirrors. *Sens Actuators A* 97–98:227–238
- Maithripala DHS, Berg JM, Dayawansa WP (2005) Control of an electrostatic microelectromechanical system using static and dynamic output feedback. *ASME J Dyn Syst Meas Control* 127(3):443–450
- ME'scope VES Operating Manual (2001) Version 3.0
- Nguyen CTC, Howe RT (1992) Quality factor control for micromechanical resonators. In: Technical digest, IEEE international electron devices meeting, San Francisco, CA, pp 505–508
- Okano Y, Hirabayashi Y (2002) Magnetically actuated micromirror and measurement system for motion characteristics using specular reflection. *IEEE J Sel Top Quantum Electron* 8(1):19–25
- Palamakumbura R, Maithripala DHS, Dayawansa WP, Inaba H (2005) Control of travelling pulses in MEMS arrays: numerical evidence of practical asymptotic stabilization. In: Proceedings of the American control conference, Portland, Oregon
- Pannu S, Chang C, Muller RS, Pisano AP (2000) Closed-loop feedback control system for improved tracking in magnetically actuated micromirrors. In: IEEE/LEOS international conference on optical MEMS, pp 107–108
- Rao SS (2004) Mechanical vibrations. Pearson Education, New Jersey
- Schweizer S, Calmes S, Laudon M, Renaud Ph (1999) Thermally actuated optical microscanner with large angle and low consumption. *Sens Actuators* 76:470–477
- Urey H (2003) Retinal scanning displays. In: Driggers R (ed) Encyclopedia of optical engineering. Marcel Dekker, New York, pp 2445–2457
- Veryeri I, Basdogan I (2007) Dynamic characterization and damping control of a MEMS structure. In: SPIE, international symposium on optomechatronic technologies, Lausanne, Switzerland
- Yalcinkaya AD, Ergenemanb O, Urey H (2007) Polymer magnetic scanners for bar code applications. *Sens Actuators A* 135:236–243